Chalcogenide Letters Vol. 18, No. 1, January 2021, p. 23 - 29

EFFECT OF Ga/Ge RATIONS ON THE STRUCTURE AND ELECTRIC PROPERTIES OF Ga–Ge–Sb–S–AgI SYSTEM

P. DONG[a,b], Q. JIAO[a,c,*], Y. ZHANG[a,b], B. MA[a,b], H. SHAN[a,b], S. DAI[a],
T. XU[a,b,c]

[a]*Laboratory of Infrared Material and Devices, Advanced Technology Research Institute, Ningbo University, Ningbo 315211, China*

[b]*Faculty of Information Science and Engineering, Ningbo University, Ningbo, 315211, China*

[c]*Ningbo Institute of Oceanography, Ningbo 315832, China*

A novel of $Ga_xGe_{(4-x)}Sb_{64}S_{128}$-40AgI glass system was prepared by melting quenching in the synthesis range of $0 \leq x \leq 4$. The structure property, thermal behavior and electrical conductivity of the prepared glasses were investigated with the different Ge/Ga ratios. From the XRD pattern, there is no crystal precipitated from the sample material, and a slightly gallium element doping induced $[GaS_4]$ tetrahedral structure units and edge-shared $[Ge(Ga)S_{(4-x)}I_x]$ mixed structure facilitated the transport of ion channels. The glass conductivity overall increased with the addition of gallium content, glass with x=1 presented the highest conductivity of 9.18×10^{-6} S/cm at room temperature. These phenomenon and results offer a new thought to explore metal-doped sulfur solid electrolytes in batteries.

(Received July 7, 2020; Accepted January 11, 2021)

Keywords: Chalcogenide glass, Structure, Solid electrolyte, Conductivity

1. Introduction

Inorganic solid electrolytes have recently attracted immense attention because of their great advantages in chemical batteries [1]. Compared with traditional liquid electrolytes, solid electrolytes not only can avoid safety issues, such as inflammability, explosiveness, and leakiness, but also transfer and guide conductive ions inhibiting the growth of lithium dendrites [2]. These electrolytes simplify the preparation process of battery and reduce its manufacturing [3]. Sulfur is essentially less electronegative than oxygen; it has less binding energy on ions, thereby allowing more free-moving ions. The radius of sulfur element is larger than that of oxygen element [4], causing the expansion of electrolyte structure and forming an enlarged ion transport channel. Therefore, sulfide solid electrolytes provide better conductive structure than oxide solid electrolytes. The solid electrolytes of sulfide system promise a good conductivity of 10−3–10−5 S/cm at room temperature. For example, Ga–Ge–S solid electrolyte has extensive glass-forming areas and provides a wide range of compositional flexibility, permitting the addition of a large number of conductive ions with less influence on its amorphous glass state. Furthermore, adding Sb into this sulfide solid electrolyte densifies the network structure, thereby improving the thermal stability of these glass systems [4,5].

In a previous research, sulfide solid electrolytes containing metal cations acted as fast ionic conductors, and the sulfur glass containing silver iodide with high ionic mobility was studied [6]. Based on the increased polarizable ability and weakness of the binding force between anions and cations, the ionic conductivity of solid electrolytes is comparable to that of commercial liquid electrolytes when the contained AgI ion conductor is converted into fast ion conductor in the α phase [6,7]. Previous experiments showed that increasing the concentration of AgI improves the

---

[*] Corresponding author: jiaoqing@nbu.edu.cn

https://doi.org/10.15251/CL.2021.181.23

ion conductivity of chalcogenide glass by several orders of magnitude. Sulfide solid electrolytes based on AgI are considered as promising solid ionic conductor materials in the development of ion batteries and one of the most reliable and stable materials [4,6,8].

In this study, a large concentration of AgI was incorporated into Ge–Ga–Sb–S solid glass electrolytes to obtain increased conductivity and keep the amorphous nature of the glass. Ga/Ge ratios were changed to optimize the ion transport channels and the network structure. On the basis of Raman spectral structure analysis, the influence of induced [GaS_4] and [$S_3Ga–GaS_3$] units on ion conductivity was discussed. The results elucidated the ion transport rules related to the electro-chemical parameters in AgI-doped sulfur solid electrolyte.

2. Experimental

Samples consisting of $Ga_xGe_{(4-x)}Sb_{64}S_{128}$-40AgI ($x = 0, 1, 2, 3, 4$) glasses were obtained via traditional melt quenching method. The elements (Ga, Ge, Sb, S, and AgI) required for the sample preparation were all with high purity (5N). Each batch was mixed in a quartz ampule with a specific stoichiometric ratio, and the preparation process was carried out in a vacuum. Each ampule weighed approximately 10 g. The sealed and evacuated ampules were kept in a rocking furnace for 24 h at a temperature of 850 °C. Then, they were quickly taken out, quenched in cold water, and fast transmitted to the annealing furnace until being annealed down to room temperature to eliminate glass stress. Afterward, all samples were incised and buffed to optical discs (10 mm in diameter and 1.7 mm in thickness) for electrical property measurements.

The amorphous nature analysis was determined using an X-ray diffraction (Bruker D2 Phaser at 30 Kv, 40 mA) with a Cu target at the range of 10 °C–70 °C with 2θ angle. Archimedes method was performed to measure the sample density. Vicker's microhardness (Hv) tests were conducted using an Everone MH3 tester with a load of 50 g. The characteristic temperature of the glass powders (10 mg) was measured via differential scanning calorimetry (DSC) on Q2000 workstation (TA, New Castle, USA, 10 °C/min) in N_2 gas atmosphere at a temperature ranging from 50 °C to 350 °C. In accordance with the measurement curves of DSC, the glass transition temperature (T_g) was determined using slope intercept method. Raman spectral photometry was conducted at 785 nm excitation wavelength to examine the sample structure (Renishaw, Gloucestershire, UK). For the AC electrical conductivity test, Au was sputtered on the polished disc surface to ensure good connection with the metal electrodes and provide the function of a block electrode. All samples were characterized by AC impedance measurements at $1.0–1 \times 10^6$ Hz frequency range using an impedance analyzer on fully automated mode, with temperature ranging from 30 °C to 100 °C. Before the detection, indium plates were added to each side of the sample to serve as current collectors.

3. Results and discussion

3.1. XRD analysis

The XRD measurement of $Ga_xGe_{(4-x)}Sb_{64}S_{128}$-40AgI ($x = 0, 1, 2, 3, 4$) glass samples are displayed in Fig. 1. The measured samples were homogeneous with deep-red color. No sharp crystallization peak appeared with the increase in Ga content. All samples were in fully amorphous nature, and an even distribution of electrochemistry was expected.

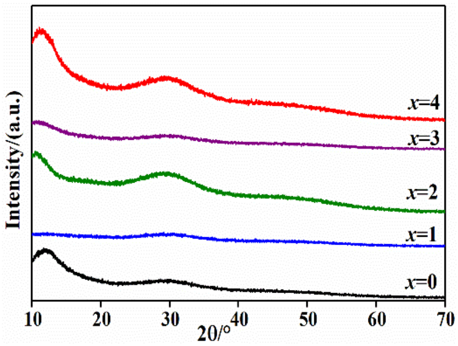

Fig. 1. XRD patterns of the prepared samples.

3.2. Physical and thermal behavior

The physical and thermal characteristics of all the samples are listed in Table 1. The glass density ρ of the samples ranged from 4.611 g/cm3 to 4.700 g/cm3 under gallium elementaddition.

Table 1. Relevant density, hardness, and thermal parameters of all glasses.

Composition	ρ (± 0.005 g/cm^3)	H_v (± 1 kg/mm^2)	T_g (± 1 °C)
x= 0	4.700	95.36	176
x= 1	4.674	97.76	180
x= 2	4.646	99.24	170
x= 3	4.624	102.10	171
x= 4	4.611	105.18	172

The atomic stacking effect and the component atomic weight generally affect the glass density. In this study, the relative atomic mass of Ge (72.64 g/mol) was higher than that of Ga (69.72 g/mol), which directly helped decrease the sample density. On the contrary, the chemical strength of Ga–S bond energy at 294 kJ/mol was higher than that of Ge–S bond energy at 265 kJ/mol [5,6,9], indicating the increase in hardness of the materials. Moreover, all samples maintained a glass transition temperature Tg of 170 °C–180 °C with stable thermal properties. This range is reasonable, indicating high connectivity of the glass network [10].

Fig. 2 demonstrates that the DSC curves were changed, with a heating rate of 10 °C /min. The dimension of glass network and the thermal stability criterion ΔT are influenced by chemical bonds and microstructure units. In this work, a slightly decreasing trend of T_g was observed with the increase of gallium content, which was possibly related to the decrease in former [GeS_4] units in the glasses. Otherwise, a part of I^- played the role of network terminal agent and prompted a broken network structure. When the addition of Ga corresponding to the [S_3Ga–I–GaS_3] unit or/and [GaS_3I] structural unit was decreased, the polymerization degree of the glass network was lost. The [GaS_3] triangles were easily transformed into [GaS_4] tetrahedral structure by the capture of free lone pair S atoms, thereby enhancing the connectivity of the glass network [10,11]. A part of I^- acted as non-bridging termination and reduced the network connectivity of the glass [5,11,12], leading to the increase in T_g first and then a slight decrease.

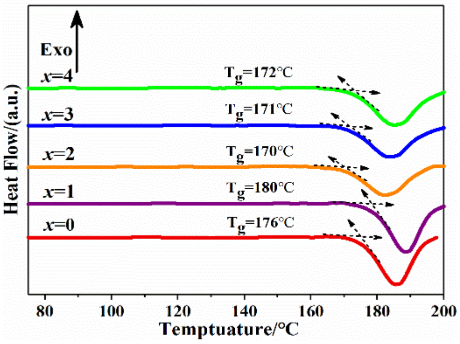

Fig. 2. DSC curves of the glasses with different Ge/Ga ratios.

3.3. Raman spectroscopy

The Raman spectra of GaxGe$_{(4\text{-}x)}$Sb$_{64}$S$_{128}$-40AgI glasses with different Ge/Ga ratios are presented in Fig. 3. The relationship between the structure of sulfur solid electrolyte and ionic conductivity was established. In the GeSbS-40AgI glass without Ga addition, the strong band at 314 cm^{-1} was associated with [SbS$_3$] pyramid units, which constructed the host framework [13,14]. The two shoulders at 265 and 340 cm^{-1} belonged to the symmetrical stretching vibrations of [GeS$_4$] units in most Ge-based glasses. The other band at 360 cm^{-1} named "companion peak" was attributed to the edge-shared [GeS$_{(4-x)}$I$_x$] mixed structure, and the three-dimensional network structure was produced by bridging the sulfur connections, the vibrations of bands near 106 cm^{-1} and 137 cm^{-1} assigned to [SbI$_3$] and [SbSI] structure units, respectively [9,10,14].

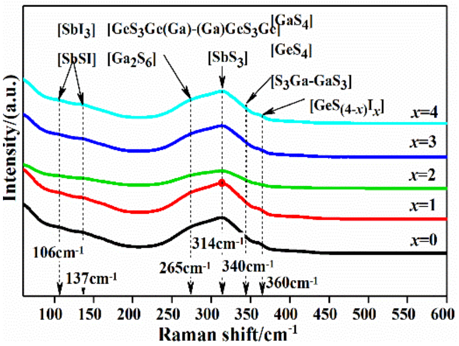

Fig. 3. Raman scattering spectra of $Ga_xGe_{(4\text{-}x)}Sb_{64}S_{128}$-40AgI bulk samples.

Replacing Ge with Ga in the network resulted in changes in the Raman spectra with a lowered vibration band at 265 cm^{-1}, indicating the formation of [S$_3$Ge(Ga)–(Ga)GeS$_3$] units. The slightly decreased intensity at 360 cm^{-1} vibration represented the replacement of Ga with Ge in the [GeS$_{(4-x)}$I$_x$] mixed structure. Meanwhile, the slight enhancement of the 340 cm^{-1} band was due to the [S$_3$Ga–GaS$_3$] ethane-like units, because [GaS$_4$] tetrahedral structure formed more easily than [S$_3$Ga–GaS$_3$] ethane-like units in chalcogenide glasses. The vibration modes of the structure units and the micro-changes in network connections modified the ion channel transport [14,15,18]. These structures provided the basic transport pathways for conductive ions with more Ga participating in the form of moved sites in the ionic channels. They also served as guidance for ionic conductivity analysis.

3.4. Ionic conductivity

The electrical properties of the Ga$_x$Ge$_{(4\text{-}x)}$Sb$_{64}$S$_{128}$-40AgI glass samples were determined using impedance spectroscopy at the temperature range of 30 °C–100 °C. The Nyquist's impedance diagrams of the samples showed the typical shape of an ionic conductor with high-frequency arc related to the conductions of the bulk matrix and low-frequency tail for the electrode interface. The typical impedance spectra are shown in Fig. 4. The value of impedance Z was calculated using the formula $Z = Z' - iZ''$ (where Z' is the real part and Z'' is the imaginary part of the impedance). The total resistance of sulfuric glass solid electrolyte could be determined by the intersection f_R of the high-frequency arc and the low-frequency tail with the horizontal line [16-19]. In the present work, the impedance showed a decreasing trend with the increase in Ga element. This finding indicated that the Ga-related network units optimized the ion transport channel and the structure sites were adjusted by the conductive net bones [Ge(Ga)S_4] and the route environment of silver ions. The irregular variation of the impedance with the increase in Ga element demonstrated the threshold of the micro-environment change in this Ge–Ga–Sb–S glass system. The ionic conductivity could be derived from the formula $\sigma = D/(A \times R)$, where D represents the sample thickness, and A represents the area of contact between the sample and the electrode. The relationship between conductivity and glass temperature usually follows the Arrhenius formula $\sigma = \sigma_0/T \exp(-Ea/KT)$, where σ_0 denotes the index factor (also called frequency factor), k represents Boltzmann constant, and T is thermodynamic temperature. Activation energy (Ea) is often defined as a temperature-independent constant. Therefore, the antiderivative of the above Arrhenius equation was obtained using the formula $\ln\sigma T = \ln\sigma_0 - Ea/kT$, and the values of Ea and σ_0 could be easily deduced from the linear regression [17-22].

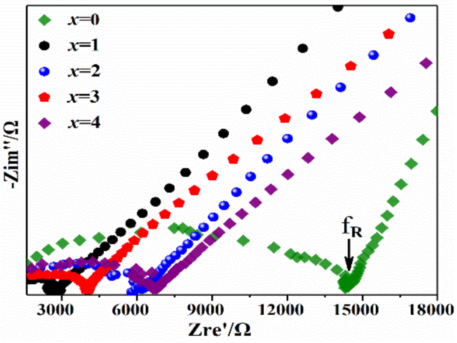

Fig. 4. Typical impedance curve with high-frequency arc and low-frequency tail of the GaxGe$_{(4-x)}$Sb$_{64}$S$_{128}$-40AgI sample at 300 K.

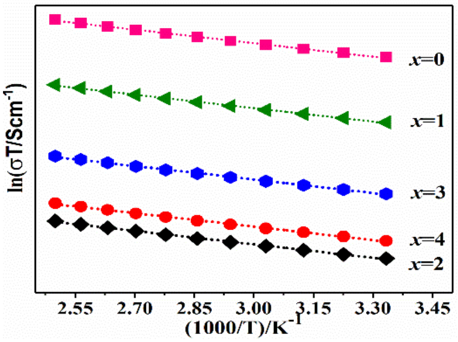

Fig. 5. Arrhenius behavior plots for bulk samples. The linear fittings of lnσT are displayed as a function of 1000/T. Open symbols represents experimental values.

Table 2. Conductivity σ_{300} and activation energy Ea dependence of Ga mole percentage.

Composition	σ_{300} (S cm^{-1})	Ea (eV)
$Ge_4Sb_{64}S_{128}$-40AgI	1.51×10^{-6}	0.029810
$GaGe_3Sb_{64}S_{128}$-40AgI	9.18×10^{-6}	0.029811
$Ga_2Ge_2Sb_{64}S_{128}$-40AgI	3.70×10^{-6}	0.029812
$Ga_3GeSb_{64}S_{128}$-40AgI	5.31×10^{-6}	0.029812
$Ga_4Sb_{64}S_{128}$-40AgI	3.23×10^{-6}	0.029812

Fig. 5 depicts a linear dependence of lnσT on 1000/T for all samples under the range of characteristic temperature. The results of σ_0 and Ea at room temperature are listed in Table 2. The ionic conductivity of the samples was almost improved by over one order of magnitude from 1.51 × 10^{-6} S/cm to 9.18 × 10^{-6} S/cm at room temperature. The maximum conductivity of the samples was approximately 9.18 × 10^{-6} S/cm. The glass not only exhibited a relatively high conductivity but also presented a decreased Ea of 0.03 eV, which was comparable to that of the bulk α-AgI (~0.05 eV) for doped glass electrolytes. This low Ea may be related to the diffusion pathway, which is based on the banding stack framework of [SbSI] structure units. When gallium was added, the resulted [GaS_4] tetrahedral structure units and edge-shared [$Ge(Ga)S_{(4-x)}I_x$] mixed structures facilitated the transport of ion channels, and the conductivity of the sample was improved. With the further increase in gallium content, large [GaS_4] tetrahedral structure units were transformed into [S_3Ga–GaS_3] ethane-like units. Moreover, the structure was unfavorable for ion channel transport, thus resulting in decreased conductivity. Considering the previous research on the GeS_4-produced the basic channels for ion transport, the modified control of Ga introduction was identified by the network rigidity change. This phenomenon suggested that adjusting the Ga/Ge proportion affected the structure of the ion transport network and influenced ionic conductivity. Analyzing the correlation between the local network structure and the ionic conductivity of $Ga_xGe_{(4-x)}Sb_{64}S_{128}$–40AgI glasses is important for new conductor materials with remarkable ionic transport properties.

4. Conclusions

In this paper, a new Ge–Ga–Sb–S–AgI sulfur-halide glass system with controlled Ga/Ge ratio was proposed. The electrical conductivity, thermal analysis, and structural characterization of the prepared samples were investigated using AC impedance method, DSC, XRD, and Raman spectroscopy. The Raman results indicated that ion conductive lines were constructed and affected by the Ge- and Ga-induced network linkages in the glass host. The results also showed that the glass electrolyte containing silver iodide provided a low Ea (0.03 eV). Under different Ge/Ga ratios, a remarkable conductivity of 9.18 × 10^{-6} S/cm was obtained with the optimal composition of $x = 1$, indicating the potential to improve the conductivity of sulfur solid electrolyte. The results offer a direction for the development of new amorphous solid conductive materials.

Acknowledgements

This work was supported by Natural National Science Foundation of China (NSFC) (Grant no. 61605093 and 51702172), National Key Research and Development Program of China (No. 2016YFB0303803 and 2016YFB0303802) and sponsored by K. C. Wong Magna Fund in Ningbo University.

References

[1] M. Tatsumisago, A. Hayashi, Journal of Non-Crystalline Solids **354**, 1411 (2008).

[2] B. Fan, H. Fu, H. Y. Li, B. Xue, X. H. Zhang, Z. K. Luo, H. L. Ma, Journal of Alloys and Compounds **740**, 61 (2018).

[3] N. Tanibata, K. Noi K, Hayashi, M. Tatsumisago, Rsc Advances **4**, 17120 (2014).

[4] D. S. Patil, M. Konale, S. Cozic, L. Calvez, V. Zima, T. Wagner, J. S. McCloy, D. Le Coq, Journal of Alloys and Compounds **782**, 375 (2019).

[5] Y. Liu, D. L. Coq, J. Ren, L. Hua, G. Chen, Journal of Non-Crystalline Solids **432**, 232 (2016).

[6] S. Cui, D. L. Coq, C. Boussard-Plédel, B. Bureau, Journal of Alloys and Compounds **639**, 173 (2015).

[7] C. Lin, Z. Zhu, J. Wang, X. Zhao, F. Chen, S. Dai, Journal of Physics and Chemistry **122**, 1486 (2018).

[8] S. Stehlik, V. Zima, T. Wagner, J. Ren, M. Frumar, Solid State Ion **179**, 1867 (2008).

[9] B. C. Ma, Q. Jiao, Y. T. Zhang, X. Sun, G. L. Yin, X. H. Zhang, H. L. Ma, X. Y. Liu, S. X. Dai, Ceramics International **46**, 6544 (2020).

[10] G. Tang, Z. Yanga, L. Luo, W. Chen, Journal of Alloys and Compounds **459**, 472 (2008).

[11] G. Tang, G. Liu, C. M. Luo, W. Chen, Journal of the American Ceramic Society **91**, 4171.

[12] H. Guo, Y. Zhai, H. Tao, Y. Gong, X. Zhao, **42**, 1111 (2007).

[13] Y. Zhang, Q. Jiao, B. Ma, C. Lin, X. Liu, S. Dai, Condensed Matter **570**, 53 (2019).

[14] A. P. Yang, M. Zhang, L. Li, Y. W. Wang, B. Zhang, Z. Y. Yang, D. Y. Tang, Journal of the American Ceramic Society **99**, 12 (2016).

[15] J. Ren, Q. Yan, T. Wagner, V. Zima, M. Frumar, B. Frumarova, G. Chen, Journal of Applied Physics **114**, 023701 (2013).

[16] J. Heo, Y. J. Min, S.-Y. Ryou, Journal of Non-Crystalline Solids **238**, 115 (1998).

[17] M. Fraenkl, B. Frumarova, V. Podzemna, S. Slang, L. Benes, M. Vlcek, T. Wagner, Journal of Non-Crystalline Solids **499**, 412 (2018).

[18] H. Z. Tao, X. J. Zhao, C. B. Jing, S. Liu, Journal of Wuhan University of Technology, 2005.

[19] Z. G. Ivanova, V. S. Vassilev, E. Cernoskova, Z. Cernosek, Journal of Physics and Chemistry of Solids **64**, 107 (2003).

[20] X. Huang, Q. Jiao, C. Lin, H. Ma, X. Zhang, E. Zhu, X. Liu, S. Dai, T. Xu, Scientific reporters **8**, 1699 (2018).

[21] Fukushima, A. Hayashi, H. Yamamura, M. Tatsumisago, Solid State Ionics **304**, 85 (2017).

[22] M. Zhao, B. Li, H. Peng, H. Yuan, J. Wei, J. Huang, Angewandte Chemie, 2019.